Chemical Physics 573 (2023) 112002

Contents lists available at ScienceDirect

Chemical Physics

journal homepage: www.elsevier.com/locate/chemphys

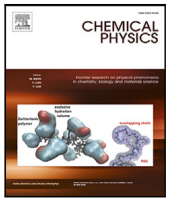

Kinetics of nanoparticle nucleation, growth, coalescence and aggregation: A theoretical study of $(Ag)_n$ nanoparticle formation based on population balance modulated by ligand binding

Mohsen Farshad[1], Jayendran Rasaiah[*,1]

Department of Chemistry, University of Maine, Orono, ME 04469, United States

ARTICLE INFO

Keywords:
Nucleation
Growth
Nanocluster
Coalescence

ABSTRACT

Understanding the mechanism of nanocluster formation during their synthesis is important in determining the different variables that govern their formation, size distributions, and stability. Here, we use the method of moments to solve the rate equations for the kinetics of metal cluster formation starting from a well-mixed solution of metal ions and reducing agents. With the incorporation of coalescence, we detected a drastic change in size distribution with a small change of a parameter – the initial ion concentration or the coalescence rate coefficient. This is a manifestation of a threshold beyond which the number of possible combinations for aggregation of clusters increases abruptly during coalescence. We observe the sensitivity of nanocluster size distribution to the coalescent growth rate and the effect of a strong ligand stabilizer in impeding coalescence.

1. Introduction

Nanoparticles are formed through many possible paths of aggregation from their constituents. This can be described mathematically by Smoluchowski's coagulation equation [1,2] if coalescence starts from the smallest species in the system which is a single atom/ion. However, in the classical LaMer mechanism [3–5], nucleation is followed by sudden aggregation of metal atoms immediately after reaching a supersaturation point where they overcome a free energy barrier for nuclei formation [6,7]. This is a consequence of the increase in attraction energies between species when the distances between them decrease following their increased local concentration. Physically, the possibility of three or more species aggregating simultaneously at the same moment is almost zero when the concentrations are very low. With the assumption that only two species can aggregate at a time, there would not be any mathematical distinction between nucleation and growth, and both follow the same principles.

In our current and previous studies on the kinetics of nanoparticle formation, we were influenced by the studies of Finke's group [8–10]. Particularly, in the original Finke–Watzky model, Finke and his group pioneered modeling a continuous nucleation process as opposed to LaMer burst nucleation and a surface autocatalytic monomeric growth mechanism. In our model, we have also incorporated the agglomeration of two species that it is usually referred to as biomolecular nucleation [11] and aggregation [12]. While we neglect the simultaneous collision of three or more particles principally, nevertheless, given the time interval of the experimental recognition, the definition of simultaneity of collision of two (such as in termolecular nucleation [13]) or more particles with a reference particle can vary from a nearly impossible or extremely rare-event to a probable event. Since we allow a specific species to undergo three growth pathways simultaneously, our model will cover higher number collisions with a given species implicitly.

In our model [14,15], nucleation is initiated by a two-body reaction where dimers are formed by aggregation of two elements [16–19]. Nevertheless, we can identify distinctive stages of nanoparticle formation, with distinguishable characteristics, as nucleation, aggregate growth, and coalescence. We can look at aggregation as a distinct stage beyond nucleation with three pathways of single monomer addition growth, single-ion addition growth, and coalescence. This perspective of incorporating different schemes into the kinetic model increases its flexibility in producing size distributions similar to those observed in experiments. For instance, the inclusion of nucleation as a distinct stage from growth allows the generation of a maximum in size distribution in our particular reaction-controlled kinetic model. The mechanism of formation of metal containing nanoparticles up to year ~2021 has been reviewed by researchers [20–22].

Experimentally, the synthesis of atomically precise ultra-small nanoparticles has come to fruition [23–33], but there is much to learn about the mechanism of nanocluster formation and their transitional

* Corresponding author.
E-mail address: rasaiah@maine.edu (J. Rasaiah).
[1] Mohsen Farshad and Jayendran C. Rasaiah worked together in completing this study.

https://doi.org/10.1016/j.chemphys.2023.112002
Received 16 March 2023; Received in revised form 14 June 2023; Accepted 17 June 2023
Available online 28 June 2023

growth to nanoparticles under various conditions. The ultra-small nanoparticles with diameters smaller than 2 nm containing less than about 200 atoms are referred to as nanoclusters. Our studies are firmly rooted in experimental studies to synthesize nanometer and sub-nanometer silver metal clusters [23–33]. Optimizing the conditions under which these nanoclusters are stable is the vital key to their synthesis. Many parameters are involved in the mechanism of nanocluster formation in a system. The initial ion and ligand concentrations and their ratio, the binding strength of ligands, and the reduction rate of ions are among the conditions that we are interested in understanding this deeply. In this regard, we have developed kinetic models by which these variables were studied systematically [14,15].

An incomplete version of our model was fitted to experimental results of silver nanoparticle formation produced from the reduction of silver nitrate by sodium borohydride in a micromixer carried out by one of the authors (MF) in which the size distribution peaked at a diameter of 0.7 nm. A spherical space of 0.7 nm in diameter can contain 10–15 silver atoms of diameter ~0.29 nm, which suggests the formation of silver nanoclusters. To overcome skepticism, we sought to understand how ultra-small silver nanoparticles could be stabilized in the early stages of growth, and the first author was motivated to undertake a theoretical study of the kinetics of the nanoparticle formation to elucidate the effect of monomeric aggregation and coalescent growth in the presence of strong and weak binding ligands. This work was done in collaboration with D.Suvlu who was another member of the second author's (Rasaiah) research group. Toward this end, we came across a kinetic study from Jensen's research group at MIT published in 2018 (Lazzari et al. [34]). We adopted their model to our interests in the kinetics of nanocluster formation, by adding more steps to increase its flexibility [14]. That is how our theoretical work on nanoclusters began—it was not some random one-point speculation in multidimensional space with no other basis.

In the earlier model, we elegantly described how the nucleation rate, ion/monomer growth rate, and ion concentration affect the final size distribution of clusters in the presence of weak and strong binding ligands [14]. However, the coalescence of clusters as a crucial pathway of nanoparticle growth was not incorporated there. The derivation of the one-dimensional (1D) coalescence rate equation by applying the method of moments on the two-dimensional (2D) equations is difficult but, in our opinion possible, and is described in this paper in the section on the Kinetic model. Nevertheless, in a later study, the effect of coalescence was studied by Suvlu et al. [15] using the original 2D equations only without invoking the method of moments, where the sensitivity of cluster size distribution to the ligand binding and coalescence in growth mechanism was discussed in detail [15]. Moreover, the high resolution of the model in comparison to the earlier model lead to the observation of distinct sizes of clusters with a subsequent particulate pattern of growth of clusters, which had been detected experimentally [35–38]. In those two models,(without and with coalescence) it was established that the high ratio of strong binding ligand to metal ion can lead to coverage of the surface of clusters with ligands that prevent the continued growth of nanoparticles. Furthermore, it was found that fast nucleation will lead to smaller clusters.

Here, we apply the method of moments to derive simplified 1D rate equations to solve the kinetic equations for the model in the presence of coalescence, as a third pathway of growth. By using the method of moments as an averaging estimator, the solution is computationally much faster and can readily be employed to follow the formation of much larger clusters. Using this method, we investigated in detail the effect of nucleation, growth pathways, ion concentration, and ligand strength on the formation of clusters. Moreover, we observed a subtle and rapid change in the size distribution of clusters with a relatively slight increase in coalescence rate or metal ion concentration from a critical point. Our model, emphasizes that precise control over the coalescence rate is a crucial step in stabilizing the small clusters. Below we describe the model and method of solution and its modification in further detail chronologically.

2. Kinetic model

The model assumes nucleation and growth stages in the presence of ligands. In this model, metal ions (M^+) can be reduced to metal atoms (M) with the rate coefficient $k_{p,1}$ (Eq. (1a)). Metal ions/atoms can associate with and dissociate from ligands (L) with rate coefficients $k_{b,1}/k_{b,2}$ and $k_{ub,2}/k_{ub,2}$ (Eq. (1b)/(1c)) respectively. Ligand-associated metal ions can reduce (ML^+) to ligand-associated metal atoms (ML) with rate coefficients $k_{p,2}$ (Eq. (1f)). Each ML^+ can dimerize with one ML and absorb an electron to form M_{2L2} dimer with rate coefficient $k_{n,ac}$ (Eq. (1e)). Dimers are also formed through self-dimerization of two ML with rate coefficient k_n (Eq. (1f)). We call, the whole process of nuclei dimer formation starting from metal ions, nucleation (Eqs. (1a) to (1e)). After the formation of nuclei, single ligand-associated metal ions/atoms can associate with and dissociate from clusters $C_{i,j}$ sequentially with rate coefficients $k_{g,ac,i,j}/k_{g,i,j}$ and $k_{d,ac,j}/k_{d,j}$ (Eqs. (1g) and (1h)). Ligands can associate with and dissociate from clusters $C_{i,j}$ with rate coefficients $k_{a,i,k}$ and $k_{e,j}$ respectively (Eq. (1i)). In autocatalytic surface nucleation/growth pathway, we assume the molecule is reduced right after reaction.

We further incorporated the coalescent growth of $C_{i,j}$ and $C_{k,l}$ clusters to form $C_{i+k,j+1}$ through Eq. (1j) of the model with rate coefficient $k_{c,i,k}$. To avoid gelation during coalescence we excluded the formation of clusters larger than a limiting size ($i+k=i_{max}$) which is a condition imposed on the model. This new constraint in the model also serves as a simple and effective remedy for the conservation of mass in the coalescence equation and enables the solutions to be obtained by the method of moments. The use of appropriately modified kernels resulted in a more accurate solution for conserving mass in Smoluchowski's coagulation equation [8,39,40]. However, we were unable to solve the equations with mass-conserving kernels due to the complexity of applying the method of moments to solve the coalescence equations. Instead, in our kinetic equations, we imposed a limit to the size of the cluster which also prevents gelation [14,15]. Furthermore, the effect of concentration of reductant in our model is mapped into the rate coefficient. Therefore, it is not explicitly implemented in our model, rather it is implicitly considered by tuning the rate coefficient. In this model, we assume following schemes:

$$M^+ \xrightarrow{k_{p,1}} M \tag{1a}$$

$$M^+ + L \underset{k_{ub,1}}{\overset{k_{b,1}}{\rightleftharpoons}} ML^+ \tag{1b}$$

$$M + L \underset{k_{ub,2}}{\overset{k_{b,2}}{\rightleftharpoons}} ML \tag{1c}$$

$$ML^+ \xrightarrow{k_{p,2}} ML \tag{1d}$$

$$ML + ML^+ \xrightarrow{k_{n,ac}} M_2L_2 \tag{1e}$$

$$ML + ML \xrightarrow{k_n} M_2L_2 \tag{1f}$$

$$C_{i,j} + ML^+ \underset{k_{d,ac,j}}{\overset{k_{g,ac,i,j}}{\rightleftharpoons}} C_{i+1,j+1} \tag{1g}$$

$$C_{i,j} + ML \underset{k_{d,j}}{\overset{k_{g,i,j}}{\rightleftharpoons}} C_{i+1,j+1} \tag{1h}$$

$$C_{i,j} + L \underset{k_{e,j}}{\overset{k_{a,i,j}}{\rightleftharpoons}} C_{i,j+1} \tag{1i}$$

$$C_{i,j} + C_{k,l} \xrightarrow{k_{c,i,k}} C_{i+k,j+1} \tag{1j}$$

$$\forall\ i \geq 2,\ \forall\ i,j \in \mathbb{N}$$

In this model of growth and ligand association to form clusters, the kinetic rate coefficients, $k_{g,ac,i,j}/k_{g,i,j}/k_{c,i,j}$ and $k_{a,i,j}$ (Eqs. (2), (3), (4), and (5)) are dependent on the number of vacant sites ($N_{s,i}-j$) on the surface of the cluster [8,14,15,40]. As before, we assume the number of sites on the cluster is dependent on the number of atoms i within

the cluster $C_{i,j}$ with $N_{s,i} = [Ai^{2/3}]$ where A = 2.08 is a scaling factor and square brackets indicate an integer [14,15,35,41–43]. On the other hand, ML, ML^+, and ligand dissociation and elimination with cluster rate coefficients, $k_{d,ac,j}$, $k_{d,j}$, and $k_{e,j}$ (Eqs. (7) and (8)) respectively, are dependent on the number of sites occupied by ligands j.

$$k_{g,ac,i,j} = k_{g,ac}(N_{s,i} - j) \tag{2}$$

$$k_{g,i,j} = k_g(N_{s,i} - j) \tag{3}$$

$$k_{c,i,k} = k_c(N_{s,i} - j)(N_{s,k} - l) \tag{4}$$

$$k_{a,i,j} = k_a(N_{s,i} - j) \tag{5}$$

$$k_{d,ac,j} = k_{d,ac}j \tag{6}$$

$$k_{d,j} = k_d j \tag{7}$$

$$k_{e,j} = k_e j \tag{8}$$

These assumed formulations for rate coefficients allow us to account for the size of the clusters $C_{i,j}$ with i number of atoms and j number of ligands covering the surface of the clusters. This means implicitly, that the growth and ligand association rate with the cluster $C_{i,j}$ increases/decreases when there is a higher/lower number of vacant sites on the cluster $C_{i,j}$. Also, the rate of ligand-associated metal ion/atom dissociation and ligand elimination from cluster $C_{i,j}$ increases/decreases when there is a higher/lower number of ligands on the surface of the cluster $C_{i,j}$.

After describing the model, we derived the rate equations for each species in the system [14,15]. Here we present the rate equation of $C_{i,j}$ with the inclusion of coalescence (Eqs. (13) and (1j)). The rate coefficients defined in Eqs. (2) to (8) are already incorporated in the rate equations.

$$\begin{aligned}\frac{d}{dt}[C_{i,j}] = &-(k_{g,ac}[ML^+] + k_g[ML])\{([C_{i,j}](N_{s,i} - j)) \\ &- [C_{i-1,j-1}](N_{s,i-1} - j + 1)\} \\ &+ (k_{d,ac} + k_d)\{[C_{i+1,j+1}](j+1)] - [C_{i,j}]j\} \\ &- k_a[L]\{[C_{i,j}](N_{s,i} - j) - [C_{i,j-1}](N_{s,i} - j + 1)\} \\ &+ k_e\{[C_{i,j+1}](j+1) - [C_{i,j}]j\} \\ &- k_c\sum_{k=2}^{i_{max}}\sum_{l=0}^{N_{s,i_{max}}}[C_{i,j}][C_{k,l}](N_{s,i} - j)(N_{s,k} - l) \\ &+ \frac{k_c}{2}\sum_{k=2}^{i-2}\sum_{l=0}^{j}[C_{i-k,j-l}][C_{k,l}](N_{s,k} - (j-l))(N_{s,i} - l)\end{aligned} \tag{9}$$

To simplify each rate equation with two internal coordinates i and j (2D) to two equations with only one internal coordinate i (1D), we averaged over the number of ligands j using method of moments [14]. Using this technique, the number of rate equations and computation cost decreases significantly. To do this, we needed the zeroth, first, and second moments formulas presented in Eqs. (10) to (12) [14,34]. Eq. (10) calculates the total concentration of clusters $[\overline{C}_i]$ with i number of atoms by summing over the concentration of $C_{i,j}$ with all the possible number of j ligands. Eq. (11) calculates the total concentration of ligands $[\overline{L}_i]$ on the clusters with i number of atoms by summing over all the possible products of j and $[C_{i,j}]$. Eq. (12) calculates $[\overline{\overline{L}}_i]$ which can provide information on the binomial distribution of the ligands on the surface of the clusters [44] by summing over all the possible products of j^2 and $[C_{i,j}]$.

$$[\overline{C}_i] = \sum_{j=0}^{N_{s,i}}[C_{i,j}] \tag{10}$$

$$[\overline{L}_i] = \sum_{j=0}^{N_{s,i}} j[C_{i,j}] \tag{11}$$

$$[\overline{\overline{L}}_i] = \sum_{j=0}^{N_{s,i}} j^2[C_{i,j}] \tag{12}$$

Table 1
Summary of rate coefficients of model.

Reaction	Rate coefficients
M^+ to M reduction	$k_{p,1}$
ML^+ to ML reduction	$k_{p,2}$
Ligand binding/unbinding of M^+ and L	$k_{b,1}/k_{ub,1}$
Ligand binding/unbinding of M and L	$k_{b,2}/k_{ub,2}$
Dimerization of $ML+$ and ML	$k_{n,ac}$
Self-dimerization of ML	k_n
ML^+ growth/dissociation	$k_{g,ac}/k_{d,ac}$
ML growth/dissociation	k_g/k_d
Ligand association/elimination	k_a/k_e
Coalescent growth	k_c

Eq. (13) for $[\overline{C}_i]$ is derived after using Eqs. (10) and (11) into Eqs. (13) and (1j) and interchanging the time derivative with summation on the left-hand side of the equation

$$\begin{aligned}\frac{d[\overline{C}_i]}{dt} = &-(k_{g,ac}[ML^+] + k_g[ML])\{([\overline{C}_i]N_{s,i} - [\overline{L}_i]) \\ &- ([\overline{C}_{i-1}]N_{s,i-1} - [\overline{L}_{i-1}])\} \\ &+ (k_{d,ac} + k_d)\{([\overline{L}_{i+1}] - [\overline{L}_i])\} \\ &- k_c([\overline{C}_i]N_{s,i} - [\overline{L}_i])\sum_{l=0}^{N_{s,i_{max}}}([\overline{C}_k]N_{s,k} - [\overline{L}_k]) \\ &+ \frac{k_c}{2}\sum_{k=2}^{i-2}([\overline{C}_{i-k}]N_{s,i-k} - [\overline{L}_{i-k}])([\overline{C}_k]N_{s,k} - [\overline{L}_k])\end{aligned} \tag{13}$$

To calculate the time dependence of the average concentration of ligands on cluster with i atoms we derived Eq. (14) by using Eqs. (13) and (1j) to (12), following a procedure similar to the derivation of Eq. (13). The details are in the supplementary information.

$$\begin{aligned}\frac{d[\overline{L}_i]}{dt} = &-(k_{g,ac}[ML^+] + k_g[ML])\{(N_{s,i}[\overline{L}_i] - [\overline{\overline{L}}_i]) \\ &- (N_{s,i-1}[\overline{C}_{i-1}] + (N_{s,i-1} - 1)[\overline{L}_{i-1}] - [\overline{\overline{L}}_{i-1}])\} \\ &+ (k_{d,ac} + k_d)\{([\overline{\overline{L}}_{i+1}] - [\overline{L}_{i+1}]) - [\overline{\overline{L}}_i]\} \\ &+ k_a[L]([\overline{C}_i]N_{s,i} - [\overline{L}_i]) - k_e[\overline{L}_i] \\ &- k_c([\overline{L}_i]N_{s,i} - [\overline{\overline{L}}_i])\sum_{k=2}^{i_{max}}([\overline{C}_k]N_{s,k} - [\overline{L}_k]) \\ &+ k_c\sum_{k=2}^{i-2}([\overline{L}_{i-k}]N_{s,i-k} - [\overline{\overline{L}}_{i-k}])([\overline{C}_k]N_{s,k} - [\overline{L}_k])\end{aligned} \tag{14}$$

After deriving the one-dimensional rate equations, we employed an ordinary differential equation (ODE) solver in MATLAB to solve the rate equations numerically under different initial conditions and rate coefficients [14]. In our calculations, we studied the effect of nucleation, growth, and initial ion concentration in presence of ligands. In Table 1, we summarize the rate coefficients used in the model. Diffusion plays no part in the kinetic rate equations for reactions in the well-mixed system.

In all the calculations, we assumed $k_{p,2} = 10^{-3}$ s^{-1}, $k_{b,1} = k_{b,2} = 10^5$ $(M\ s)^{-1}$, $k_{ub,1}/k_{ub,2} = 10^{-7}$ $(M\ s)^{-1}$, $k_{d,ac} = k_d = 10^{-9}$ $(M\ s)^{-1}$, and $k_e = 10^3$ $(M\ s)^{-1}$. The remaining rate coefficients vary in different calculations. Moreover, the initial concentration of ligand (L) was set to 6.0 mM throughout all the calculations, as in previous calculations.

3. Results

To understand the effect of nucleation rate on the size distribution of clusters, we varied the rate coefficients ($k_{p,1}$) and (k_n, $k_{n,ac}$) for monomer and dimer formation respectively in the presence of strong and weak binding ligands. Fig. 1 shows that fast nucleation promotes the formation of smaller clusters [14,45].

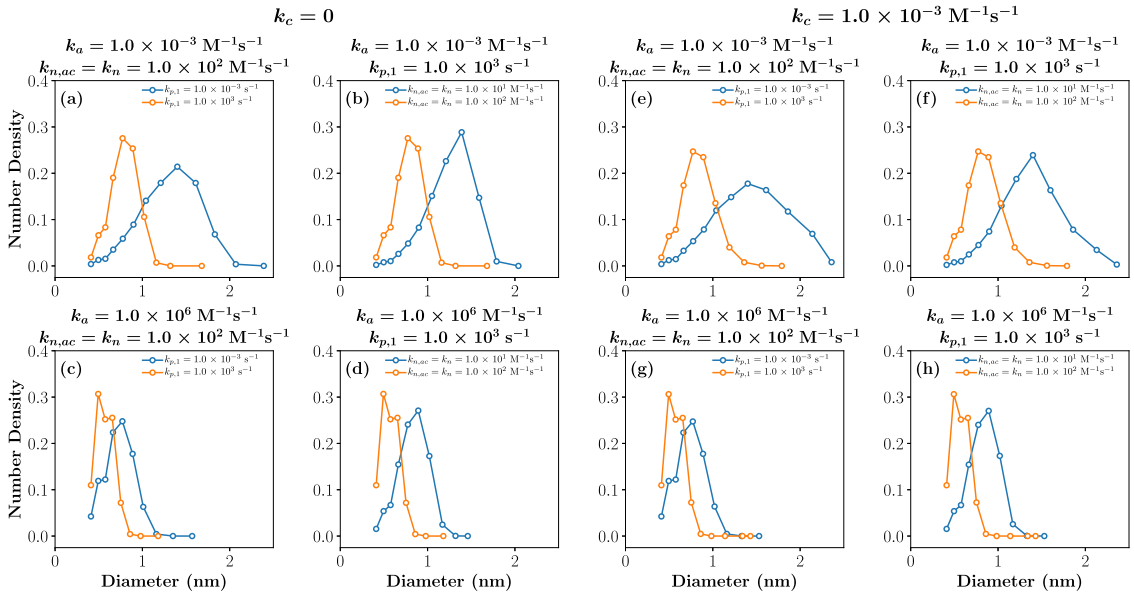

Fig. 1. Effect of nucleation rate on the final size distribution of clusters in absence (a–d) and presence (e–h) of coalescent growth pathway. (a, c) The effect of precursor to bare monomer formation rate coefficient, $k_{p,1}$, on the size distribution of clusters in the presence of weak and strong ligands. (b, d) The effect of nuclei formation rate coefficients, k_n and $k_{n,ac}$, on the size distribution of clusters in the presence of weak and strong ligands respectively. (e, g) are figures corresponding to (a, c) but when the coalescence rate $k_c = 10^{-3}$ (M s)$^{-1}$.

The figure clearly shows the presence of ultra-small nanoparticles with diameters around 0.7 nm in agreement with the results of mixing experiments [23–33]. Large values of the kinetic coefficient $k_{p,1}$ represent a strong reducing agent which leads to fast monomer formation (SI Appendix, Figs. S1 to S4), with simultaneous reduction of ions, when the final size of clusters decreases as monomer formation is part of the nucleation process. Similarly, large k_n and $k_{n,ac}$ rate coefficients for dimerizations simultaneously increase nucleation which leads to the formation of smaller clusters (SI Appendix, Figs. S1 and S2). Comparing Figs. 1a and 1b with Figs. 1e and 1, we see that the size of clusters increases considerably with the inclusion of a slow coalescence rate coefficient, $k_c = 10^{-3}$ (M s)$^{-1}$ rather than zero. The distribution of clusters in presence of strong binding ligands does not change noticeably from when coalescence rate is zero (Figs. 1c and 1d) to when a slow coalescence rate coefficient is implemented in the calculations (Figs. 1a and 1b). This comparison illustrates the sensitivity of cluster formation to the coalescent growth pathway, and how it can be prevented with strong capping agents [15,46].

After investigating the effect of nucleation on cluster size we sought to understand and compare the effect of ion (ML^+) and atom (ML) addition growth pathways on the size distributions of clusters in the presence of slow coalescent growth rates. Our results in Figs. 1a, 1b, and SI Appendix, Fig. S5 show that in the presence of an ion additional growth pathway leads to slightly smaller clusters for different $k_{g,ac}$ rate coefficients in comparison to ML addition growth pathway with corresponding k_g rate coefficients when precursor and dimerization rate coefficients are $k_{p,1} = 10^3$ s^{-1} (fast reduction rate) and $k_{n,ac} = k_n = 10^2$ (M s)$^{-1}$ (relatively faster dimerization) respectively. On the other hand, Figs. 2c, 2d, and SI Appendix, Fig. S6 show that when precursor rate coefficient is slow ($k_{p,1} = 10^{-3}$ s^{-1}), ML^+ additional growth pathway for large $k_{g,ac}$ rate coefficients leads to the formation of larger clusters with wider distributions in comparison to corresponding size distributions in ML growth pathway. For $k_{n,ac} = k_n = 10^1$ (M s)$^{-1}$ (relatively slower dimerization) with either $k_{p,1} = 10^3$ or $k_{p,1} = 10^{-3}$ s^{-1} (fast or slow reduction rates) in presence of either weak or strong stabilizing ligands the ML^+ additional pathway usually results in slightly smaller clusters for different growth rate coefficients in comparison to ML growth pathway (SI Appendix, Figs. S7 to S12).

In the ion addition growth pathway, ML monomers are only involved in nuclei dimer formation. However, ML^+ ions are consumed

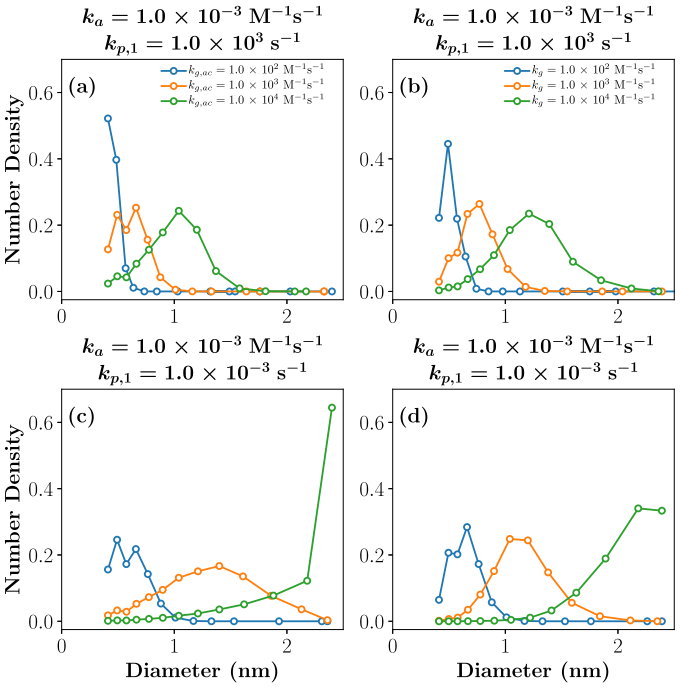

Fig. 2. Effect of ligand-associated ion (a, c) and monomer (b, d) addition growth rate on the final size distribution of clusters in presence of fast (a, b) and slow (c, d) reducing agents. For these sets of calculations $k_n = 10^2$ (M s)$^{-1}$.

through both dimerization and growth. Therefore, a significant portion of ML population remains as single monomers in the system when a high population of ML monomers is generated with a strong reducing agent. As a result, size distributions of clusters in the ion growth pathway (Fig. 2a) are relatively smaller in comparison to size distributions of clusters in the atom growth pathway (Fig. 2c). With a slow reducing agent, on the other hand, there will be enough ML^+ to proceed with the growth of clusters for the ion addition pathway. Also, the number of ML remainder will be extremely low as most of them are consumed rapidly

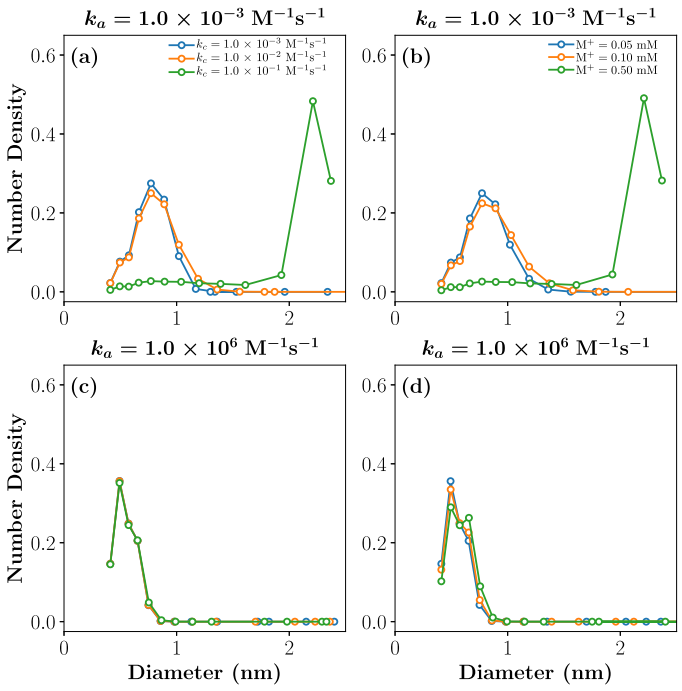

Fig. 3. Effect of coalescent growth rate (a, c) and ion concentration (b, d) on the final size distribution of clusters in the presence of weak ligands (a, b) and strong ligands (c, d).

during dimerization with a high population of ML^+ when the reduction rate is slow [47]. Consequently, wider and larger distributions are observed in the ion growth pathway (Fig. 2b) in presence of a slow reducing agent compared with the monomer growth pathway (Fig. 2d).

In Figs. 1e and 1f, we observed the sensitivity of cluster sizes to the coalescent growth rate where a small value of k_c increased the width of the size distribution of clusters significantly in presence of weak binding ligands. To confirm the importance of coalescent growth in the formation of clusters, we calculated the size distribution of clusters with different values of k_c. Fig. 3a shows that when k_c increases from 10^{-4} $(M\ s)^{-1}$ to 10^{-3} $(M\ s)^{-1}$ size distribution of particles only shifts slightly to larger particles indicating an insufficient rate for coalescence. The size distribution of clusters suddenly shifts to larger clusters when k_c increases to 10^{-3} as if the coalescent rate has passed a threshold (Fig. 4). This implies the number of combinations for growth increases substantially with the increase of coalescence rate coefficient by a factor of one, confirming the sensitivity of size distribution of clusters to coalescence. Fig. 3b shows that strong binding ligands stop the coalescence of clusters and stabilize them in their earliest stages of growth under certain conditions as found earlier (Fig. 4) [15].

Fig. 4 shows the time evolution of species in the system with different initial ion concentrations in presence of weak and strong ligands which are associated with Figs. 3a and 3c respectively.

Once we understood the effect of nucleation and growth pathways on the size distribution of clusters, we wanted to understand the effect of initial ion metal concentration on the size distribution of clusters. Therefore, we varied the initial concentration of metal ions from 0.05 up to 0.5 mM. Fig. 3b shows a sudden change in the size distribution of clusters in presence of weak binding ligands when the initial metal ion concentration increased to 0.5 mM (Fig. 5). The threshold is evident here too, similar to the subtle change in the size distribution of clusters that were observed with relatively larger coalescence rate coefficients. Again, this is due to the sudden increase of the coalescent rate when there are more ions/atoms/clusters involved with the growth mechanism in the system. Fig. 3d shows that strong binding ligands again stabilize the clusters in the early stages of growth regardless of initial concentration of metal ions, and the average size of clusters only increases slightly with the increase of concentration (Fig. 5).

Fig. 5 shows the time evolution of species in the system with different coalescence rate coefficients in presence of weak and strong ligands which is associated with Figs. 3b and 3d respectively.

4. Discussion

Finding the optimal condition for the synthesis of ultra-small nanoparticles in experiments is challenging as the instrumental techniques are not sufficiently advanced to monitor the aggregation of species in the system with high resolution and short time frames. Searching for deterministic conditions ultimately increases the reaction efficacy and reduces the experimental costs. Theoretical models unveil the significance of circumstances that lead to the formation of nanoclusters and their transition to nanoparticles. Using various kinetic models [14,15,34,41,43,48–53], the effect of many variables on the size distribution of clusters is well understood. We mechanistically further dig into the nanocluster formation to understand how fast nucleation, slow growth, strong ligands, and high ratio of ion concentration to ligand decreases the size of the clusters that are formed.

We showed that fast precursor conversion to metal atom and dimer formation simultaneously increase nucleation. Consequently, growth occurs evenly through all the nuclei and subsequent seed clusters. This means the constituents in the system aggregate at an approximately uniform rate which results in relatively monodispersed smaller clusters. Fig. 6 visually describes how fast and slow nucleation, sequentially, results in high and low uniform distribution of seed clusters which are the

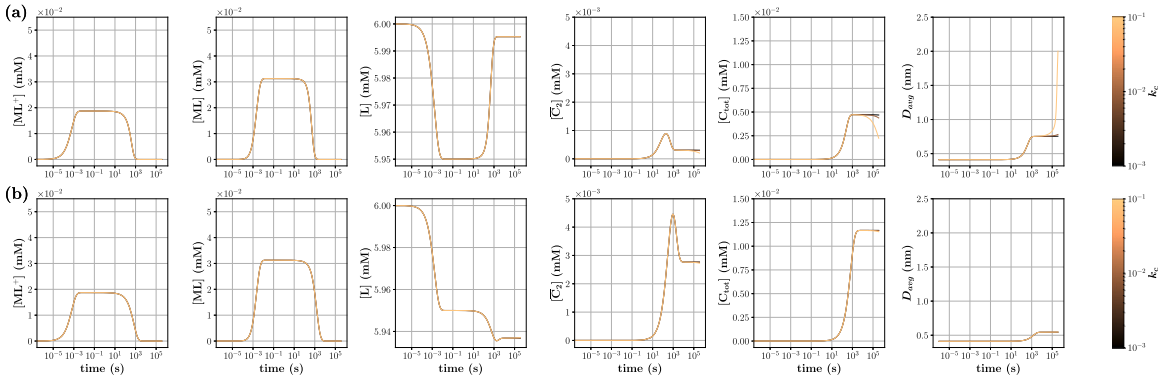

Fig. 4. Time evolution of species in the system for k_c rate coefficients in presence of (a) weak and (b) strong stabilizing ligands. The rate coefficients for weak and strong ligands are $k_a = 10^{-3}$ $(M\ s)^{-1}$ and $k_a = 10^{6}$ $(M\ s)^{-1}$ respectively. C_{tot} represents the total concentration of clusters in the system.

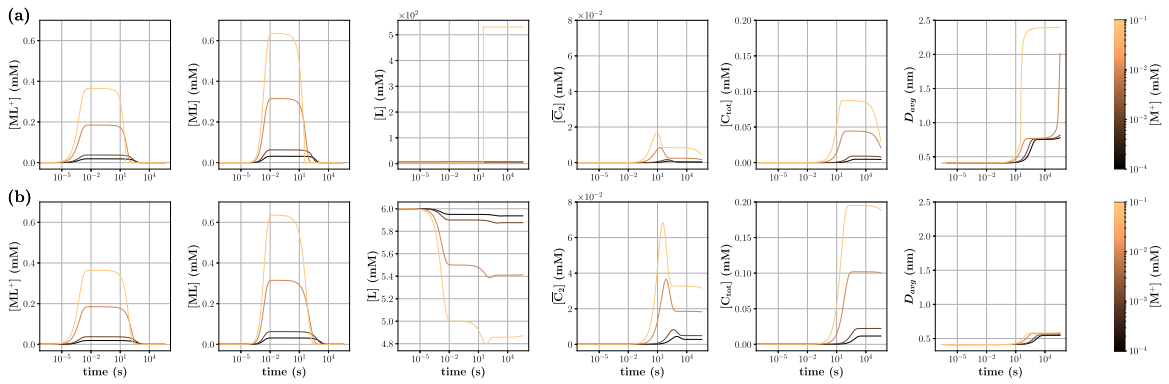

Fig. 5. Time evolution of species in the system with different initial concentrations of metal ion with $k_c = 10^{-3}$ rate coefficient in presence of (a) weak and (b) strong stabilizing ligand. The rate coefficients for weak and strong ligands are $k_a = 10^{-3}$ (M s)$^{-1}$ and $k_a = 10^{6}$ (M s)$^{-1}$ respectively. C_{tot} represents the total concentration of clusters in the system.

foundations of smaller and larger clusters respectively through growth. Simultaneous nucleation leads to the formation of a high number of nuclei at the same time, and consequently, uniform consumption of ions/atoms and small clusters [5,7,54].

Furthermore, as expected, a slow growth rate decreases the size of clusters. The solutions to the rate equations of our model displayed here show that the ion addition growth pathway can generate both larger or smaller distribution of clusters in comparison to the atom addition growth pathway under different conditions which makes it complicated to interpret their nucleation and growth mechanisms. It is evident that with slow precursor conversion, there will be a high number of ML+ ions in the system which devours the low number of ML monomers through dimerization in the ion addition growth pathway. This must lead to relatively faster nucleation and formation of smaller clusters in the ion addition pathway in comparison to the atom growth pathway with a low concentration of ML for self-dimerization. However, with a fast single ion growth rate, the nucleation rate can decrease, because nucleation competes with growth in utilizing the ions. The same scenario can be true for a single monomer growth pathway, but there would be less competition between nucleation and growth for the consumption of monomers in this pathway. The total population of ML for the atom growth pathway is significantly larger than the total population of ML^+ for the ion growth pathway in our model. With a fast reduction rate in the ion growth pathway, there will be significantly less number of ML^+ ions for the growth of seed clusters and many single (ML) monomers are left in the system. In contrast, in the atom growth pathway, almost all the population of ML is consumed through dimerization and monomer addition growth.

With the inclusion of coalescent growth in the model, we have confirmed the high sensitivity of cluster sizes to the extent of coalescence [7,51,55–59]. A threshold point in transitional growth of nanoclusters to nanoparticles was evident when we changed the coalescent growth rate or initial ion concentration (Fig. 6). Beyond this point, the cluster grows to maximum sizes, because the number of combinations in coalescing species increases steeply with the growth of clusters. Consequently, we observed a sudden increase in the size distribution of clusters when coalescence rate coefficient or ion concentration passes a certain point (Fig. 6). We further found that strong ligands can stop the coalescent growth pathway more than other growth pathways (Fig. 3). For coalescence of clusters, more ligands need to be eliminated from the surface of the clusters whereas in a single monomer/ion growth pathway one vacant site on the cluster is enough. Strong ligands have high adherence to the surface of clusters that prevent the aggregation of other species to the clusters, as manifested in our purely reaction-limited kinetic model.

Our study further provides information on how ligand strength can impede the growth of clusters. Therefore, we expect the choice of a weak ligand such as phosphine relative to a stronger ligand such as thiolate, when the other conditions are the same, can lead to the formation of larger particles. As shown in our model, a subtle change in a parameter such as ion concentration or coalescence rate coefficient can cause particles to either remain small or grow to larger nanoparticles as observed in different experiments. Last but not least, this model can be extended to study systems containing different types of ligands, both weak and strong for instance such as thiolate and phosphine ligands respectively with Au^+. Principally, one may anticipate the formation of a bimodal distribution of clusters as growth will occur with two different scenarios. The determination of the size distribution of the larger or smaller clusters requires a detailed investigation under given conditions, whether one dominates the other or both populations are balanced closely with each other.

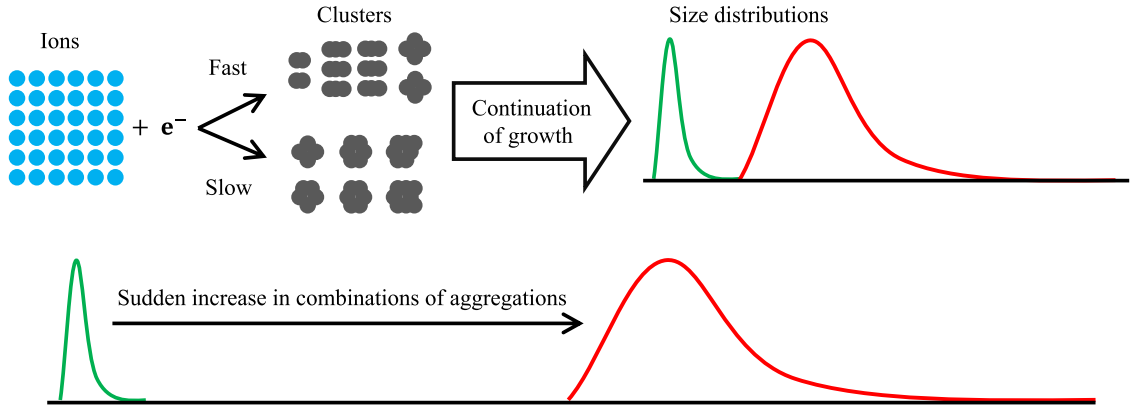

Fig. 6. Schematic illustration of the size distributions with slow and fast nucleation and growth. Also a schematic illustration of the sudden increase in the number of combinations of aggregation of clusters during coalescence triggered by a small change of a parameter such as initial ion concentration or coalescent rate coefficient in the system.

5. Conclusions

Strong ligands favor the formation of nanoclusters. In the presence of weak ligands, the range of optimal conditions for the formation of sub-nano- and nano-clusters is limited even when coalescent growth is neglected. The range of conditions that lead to the formation of ultra-small nanoparticles is further narrowed when a coalescent growth pathway is included. A sudden change in the size distribution of clusters with a small change in coalescence rate or ion concentration in the system indicates a drastic change in the number of aggregation combinations through coalescence. However, when strong binding ligands are present in the system, the range of conditions that lead to the formation of ultra-small nanoparticles increases as it hinders the growth mechanism. Ligands that cover the surface of metal clusters prevent the addition of another species to the clusters. Our calculations show that the coalescence is more sensitive to ligands than the ion/atom addition growth pathways because for coalescence to occur more ligands are required to dissociate from the surface. We further attest that fast nucleation leads to the smaller and narrower size distribution of clusters as it increases the uniformity of the nucleation and growth. Our calculations explain the experimental conditions under which ultra-small nanoparticles or so-called subnanometer metal nanoclusters can be synthesized in well-mixed solutions. The kinetic rate equations which include coalescence are relatively easy to solve for different initial concentrations of metal ion solutions and rate coefficients accounting for the strength of the reducing agents, binding ligands, and the rates of growth and coalescence. This should be valuable in designing experiments to synthesize and study nanometer and subnanometer metal clusters.

Declaration of competing interest

The authors declare that they have no known competing financial interests or personal relationships that could have appeared to influence the work reported in this paper.

Data availability

Data will be made available on request.

Acknowledgments

We thank the Advanced Computing Group of the University of Maine System, in particular Stephen Cousins for his continuous support in providing us with computer time. We thank Dylan Suvlu for his contributions to and interest in developing the model described in this work. The computer resources used in this study were supported by an NSF grant CC* Comp High-Memory Computer Resources for Maine, Award Number: 2018851

Appendix A. Supplementary data

Supplementary material related to this article can be found online at https://doi.org/10.1016/j.chemphys.2023.112002. We described in detail the derivation of zeroth and first moments of coalescence terms in the rate equation. We also include Figures S1–S12 in the Supporting Information.

References

[1] M.V. Smoluchowski, Über Brownsche Molekularbewegung unter Einwirkung äußerer Kräfte und deren Zusammenhang mit der verallgemeinerten Diffusionsgleichung, Ann. Phys. 353 (24) (1916) 1103–1112.
[2] D.J. Aldous, Deterministic and stochastic models for coalescence (aggregation and coagulation): A review of the mean-field theory for probabilists, Bernoulli 5 (1) (1999) 3.
[3] V.K. LaMer, R.H. Dinegar, Theory, production and mechanism of formation of monodispersed hydrosols, J. Am. Chem. Soc. 72 (11) (1950) 4847–4854.
[4] M.A. Watzky, R.G. Finke, Transition metal nanocluster formation kinetic and mechanistic studies. A new mechanism when hydrogen is the reductant: Slow, continuous nucleation and fast autocatalytic surface growth, J. Am. Chem. Soc. 119 (43) (1997) 10382–10400.
[5] N.T.K. Thanh, N. Maclean, S. Mahiddine, Mechanisms of nucleation and growth of nanoparticles in solution, Chem. Rev. 114 (15) (2014) 7610–7630.
[6] R. Becker, W. Döring, Kinetische Behandlung der Keimbildung in übersättigten Dämpfen, Ann. Phys. 416 (8) (1935) 719–752.
[7] J. Polte, Fundamental growth principles of colloidal metal nanoparticles – a new perspective, CrystEngComm 17 (36) (2015) 6809–6830.
[8] D.R. Handwerk, P.D. Shipman, C.B. Whitehead, S. Özkar, R.G. Finke, Mechanism-enabled population balance modeling of particle formation en route to particle average size and size distribution understanding and control, J. Am. Chem. Soc. 141 (40) (2019) 15827–15839.
[9] C.B. Whitehead, R.G. Finke, Particle formation mechanisms supported by *in situ* synchrotron XAFS and SAXS studies: a review of metal, metal-oxide, semiconductor and selected other nanoparticle formation reactions, Mater. Adv. 2 (20) (2021) 6532–6568.
[10] D.K. Long, W. Bangerth, D.R. Handwerk, C.B. Whitehead, P.D. Shipman, R.G. Finke, Estimating reaction parameters in mechanism-enabled population balance models of nanoparticle size distributions: A Bayesian inverse problem approach, J. Comput. Chem. 43 (1) (2022) 43–56.
[11] W.W. Laxson, R.G. Finke, Nucleation is second order: An apparent kinetically effective nucleus of two for Ir(0) nNanoparticle formation from [(1,5-COD)Ir I·P 2W 15Nb 3O 62] 8–Plus hydrogen, J. Am. Chem. Soc. 136 (50) (2014-12-04) 17601–17615.
[12] B.J. Hornstein, R.G. Finke, Transition-metal nanocluster kinetic and mechanistic studies emphasizing nanocluster agglomeration: Demonstration of a kinetic method that allows monitoring of all three phasescof nanocluster formation and aging, Chem. Mater. 16 (1) (2004-01-01) 139–150.
[13] S. Özkar, R.G. Finke, Silver nanoparticles synthesized by microwave heating: A kinetic and mechanistic re-analysis and re-interpretation, J. Phys. Chem. C 121 (49) (2017) 27643–27654.
[14] M. Farshad, D. Suvlu, J.C. Rasaiah, Ligand-mediated nanocluster formation with classical and autocatalytic growth, J. Phys. Chem. C 123 (49) (2019) 29954–29963.
[15] D. Suvlu, M. Farshad, J.C. Rasaiah, Nanocluster growth and coalescence modulated by ligands, J. Phys. Chem. C 124 (31) (2020) 17340–17346.
[16] K.G. Stamplecoskie, J.C. Scaiano, Kinetics of the formation of silver dimers: early stages in the formation of silver nanoparticles, J. Am. Chem. Soc. 133 (11) (2011) 3913–3920.
[17] A. Henglein, Small-particle research: physicochemical properties of extremely small colloidal metal and semiconductor particles, Chem. Rev. 89 (8) (1989) 1861–1873.
[18] M. Mostafavi, G.R. Dey, L. François, J. Belloni, Transient and stable silver clusters induced by radiolysis in methanol, J. Phys. Chem. A 106 (43) (2002-10-01) 10184–10194.
[19] J. Belloni, J.-L. Marignier, M. Mostafavi, Mechanisms of metal nanoparticles nucleation and growth studied by radiolysis, Radiat. Phys. Chem. 169 (2020) 107952.
[20] V.I. Irzhak, The mechanisms of the formation of metal-containing nanoparticles, Rev. J. Chem. 6 (4) (2016) 370–404.
[21] C.B. Whitehead, S. Özkar, R.G. Finke, LaMer's 1950 model for particle formation of instantaneous nucleation and diffusion-controlled growth: A historical look at the model's origins, assumptions, equations, and underlying sulfur sol formation kinetics data, Chem. Mater. 31 (18) (2019) 7116–7132.
[22] C.B. Whitehead, S. Özkar, R.G. Finke, LaMer's 1950 model of particle formation: a review and critical analysis of its classical nucleation and fluctuation theory basis, of competing models and mechanisms for phase-changes and particle formation, and then of its application to silver halide, semiconductor, metal, and metal-oxide nanoparticles, Mater. Adv. 2 (1) (2021) 186–235.
[23] R. Jin, Quantum sized, thiolate-protected gold nanoclusters, Nanoscale 2 (3) (2010) 343–362.
[24] R. Jin, H. Qian, Z. Wu, Y. Zhu, M. Zhu, A. Mohanty, N. Garg, Size focusing: A methodology for synthesizing atomically precise gold nanoclusters, J. Phys. Chem. Lett. 1 (19) (2010) 2903–2910.
[25] Y. Lu, W. Chen, Sub-nanometre sized metal clusters: from synthetic challenges to the unique property discoveries, Chem. Soc. Rev. 41 (9) (2012) 3594–3623.
[26] R. Jin, Atomically precise metal nanoclusters: stable sizes and optical properties, Nanoscale 7 (5) (2015) 1549–1565.
[27] R. Jin, C. Zeng, M. Zhou, Y. Chen, Atomically precise colloidal metal nanoclusters and nanoparticles: Fundamentals and opportunities, Chem. Rev. 116 (18) (2016) 10346–10413.

[28] J. Fang, B. Zhang, Q. Yao, Y. Yang, J. Xie, N. Yan, Recent advances in the synthesis and catalytic applications of ligand-protected, atomically precise metal nanoclusters, Coord. Chem. Rev. 322 (2016) 1–29.
[29] I. Chakraborty, T. Pradeep, Atomically precise clusters of noble metals: Emerging link between atoms and nanoparticles, Chem. Rev. 117 (12) (2017) 8208–8271.
[30] Q. Yao, T. Chen, X. Yuan, J. Xie, Toward total synthesis of thiolate-protected metal nanoclusters, Acc. Chem. Res. 51 (6) (2018) 1338–1348.
[31] K. Yonesato, H. Ito, H. Itakura, D. Yokogawa, T. Kikuchi, N. Mizuno, K. Yamaguchi, K. Suzuki, Controlled assembly synthesis of atomically precise ultrastable silver nanoclusters with polyoxometalates, J. Am. Chem. Soc. 141 (50) (2019) 19550–19554.
[32] X. Du, R. Jin, Atomic-precision engineering of metal nanoclusters, Dalton Trans. 49 (31) (2020) 10701–10707.
[33] M.A. Moyet, M.R. Hossen, A. Ward, O. Adams, M.D. Mason, S.D. Collins, R.L. Smith, MEMS micromixer for ultra fast mixing of fluids, in: 2020 IEEE 33rd International Conference on Micro Electro Mechanical Systems, MEMS, IEEE, Vancouver, BC, Canada, 2020, pp. 1137–1140.
[34] S. Lazzari, P.M. Theiler, Y. Shen, C.W. Coley, A. Stemmer, K.F. Jensen, Ligand-mediated nanocrystal growth, Langmuir 34 (10) (2018) 3307–3315.
[35] A. Dass, Nano-scaling law: geometric foundation of thiolated gold nanomolecules, Nanoscale 4 (7) (2012) 2260.
[36] Y. Negishi, K. Nobusada, T. Tsukuda, Glutathione-protected gold clusters revisited: Bridging the gap between gold(I)—thiolate complexes and thiolate-protected gold nanocrystals, J. Am. Chem. Soc. 127 (14) (2005) 5261–5270.
[37] C. Zeng, Y. Chen, K. Iida, K. Nobusada, K. Kirschbaum, K.J. Lambright, R. Jin, Gold quantum boxes: On the periodicities and the quantum confinement in the Au28, Au36, Au44, and Au52 magic series, J. Am. Chem. Soc. 138 (12) (2016) 3950–3953.
[38] Q. Yao, X. Yuan, V. Fung, Y. Yu, D.T. Leong, D.-e. Jiang, J. Xie, Understanding seed-mediated growth of gold nanoclusters at molecular level, Nature Commun. 8 (1) (2017) 927.
[39] J.R. Norris, Smoluchowski's coagulation equation: uniqueness, nonuniqueness and a hydrodynamic limit for the stochastic coalescent, Ann. Appl. Probab. 9 (1) (1999) 78–109.
[40] S. Mozaffari, W. Li, C. Thompson, S. Ivanov, S. Seifert, B. Lee, L. Kovarik, A.M. Karim, Ligand-mediated nucleation and growth of palladium metal nanoparticles, J. Vis. Exp. JoVE (136) (2018-06-25).
[41] S. Lazzari, L. Nicoud, B. Jaquet, M. Lattuada, M. Morbidelli, Fractal-like structures in colloid science, Adv. Colloid Interface Sci. 235 (2016) 1–13.
[42] S. Mozaffari, W. Li, C. Thompson, S. Ivanov, S. Seifert, B. Lee, L. Kovarik, A.M. Karim, Colloidal nanoparticle size control: Experimental and kinetic modeling investigation of the ligand-metal binding role in controlling the nucleation and growth kinetics, Nanoscale 9 (36) (2017-09-21) 13772–13785.
[43] S. Mozaffari, W. Li, C. Thompson, S. Ivanov, S. Seifert, B. Lee, L. Kovarik, A.M. Karim, Ligand-mediated nucleation and growth of palladium metal nanoparticles, J. Vis. Exp. JoVE (136) (2018).
[44] A.J. Morris-Cohen, V. Vasilenko, V.A. Amin, M.G. Reuter, E.A. Weiss, Model for adsorption of ligands to colloidal quantum dots with concentration-dependent surface structure, ACS Nano 6 (1) (2012) 557–565.
[45] P.G. Vekilov, Nucleation, Cryst. Growth Des. 10 (12) (2010) 5007–5019.
[46] M.G. Taylor, G. Mpourmpakis, Thermodynamic stability of ligand-protected metal nanoclusters, Nature Commun. 8 (1) (2017) 15988.
[47] M. Farshad, D.C. Perera, J.C. Rasaiah, Theoretical study of the stability, structure, and optical spectra of small silver clusters and their formation using density functional theory, Phys. Chem. Chem. Phys. 23 (45) (2021) 25507–25517.
[48] S. Mozaffari, W. Li, C. Thompson, S. Ivanov, S. Seifert, B. Lee, L. Kovarik, A.M. Karim, Colloidal nanoparticle size control: experimental and kinetic modeling investigation of the ligand-metal binding role in controlling the nucleation and growth kinetics, Nanoscale 9 (36) (2017) 13772–13785.
[49] S. Lazzari, M. Abolhasani, K.F. Jensen, Modeling of the formation kinetics and size distribution evolution of II–VI quantum dots, React. Chem. Eng. 2 (4) (2017) 567–576.
[50] E.E. Finney, R.G. Finke, Nanocluster nucleation and growth kinetic and mechanistic studies: a review emphasizing transition-metal nanoclusters, J. Colloid Interface Sci. 317 (2) (2008) 351–374.
[51] E.E. Finney, R.G. Finke, The four-step, double-autocatalytic mechanism for transition-metal nanocluster nucleation, growth, and then agglomeration: Metal, ligand, concentration, temperature, and solvent dependency studies, Chem. Mater. 20 (5) (2008) 1956–1970.
[52] E.E. Finney, R.G. Finke, Is there a minimal chemical mechanism underlying classical Avrami-Erofe'ev treatments of phase-transformation kinetic data? Chem. Mater. 21 (19) (2009) 4692–4705.
[53] M.A. Watzky, R.G. Finke, Gold nanoparticle formation kinetics and mechanism: A critical analysis of the "redox crystallization" mechanism, ACS Omega 3 (2) (2018) 1555–1563.
[54] A. Mahata, M.A. Zaeem, M.I. Baskes, Understanding homogeneous nucleation in solidification of aluminum by molecular dynamics simulations, Modelling Simul. Mater. Sci. Eng. 26 (2) (2018) 025007.
[55] H. Zheng, R.K. Smith, Y.w. Jun, C. Kisielowski, U. Dahmen, A.P. Alivisatos, Observation of single colloidal platinum nanocrystal growth trajectories, Science 324 (5932) (2009) 1309–1312.
[56] M. Takesue, T. Tomura, M. Yamada, K. Hata, S. Kuwamoto, T. Yonezawa, Size of elementary clusters and process period in silver nanoparticle formation, J. Am. Chem. Soc. 133 (36) (2011) 14164–14167.
[57] F. Wang, V.N. Richards, S.P. Shields, W.E. Buhro, Kinetics and mechanisms of aggregative nanocrystal growth, Chem. Mater. 26 (1) (2013) 5–21.
[58] C. Besson, E.E. Finney, R.G. Finke, Nanocluster Nucleation, Growth, and Then Agglomeration Kinetic and Mechanistic Studies: A More General, Four-Step Mechanism Involving Double Autocatalysis, Chem. Mater. 17 (20) (2005) 4925–4938.
[59] C. Besson, E.E. Finney, R.G. Finke, A mechanism for transition-metal nanoparticle self-assembly, J. Am. Chem. Soc. 127 (22) (2005) 8179–8184.